


Acoustic Nanoparticle Trapping Is Driven by Synergy between Acoustic and Hydrodynamic Interactions

Alen Pavlič^{*} and Thierry Baasch[†]

*Division of Chemistry and Chemical Engineering, California Institute of Technology, Pasadena, California, USA
and Department of Biomedical Engineering, Lund University, Lund, Sweden*

 (Received 4 June 2025; revised 10 September 2025; accepted 15 September 2025; published 28 October 2025)

Acoustic forces occurring in resonant microfluidic chambers allow the handling of micrometer-sized particles. Trapping of nanoparticles has been shown for high particle concentrations and after preseeding the chamber with larger particles. We show that the trapping mechanism is due to synergy between hydrodynamic shielding and acoustic forces. Acoustic interactions are significant only when seed particles are involved and are negligible when trapping monodisperse particles. Density-selective nanoparticle trapping is suggested based on the numerical results.

DOI: [10.1103/6l7z-bjzy](https://doi.org/10.1103/6l7z-bjzy)

Acoustic fields allow trapping of micrometer and submicrometer biological material such as cells [1,2], cell-laden hydrogel droplets [3], bacteria [4,5], and vesicles [6–11] as well as the trapping of low-concentration microplastics [12,13] against an external flow. The trapped material is thereby isolated and enriched, which enables studying rare biological materials. Although acoustic trapping is a key technology for the acoustic manipulation of submicron particles, the underlying mechanism is not well understood. In this Letter, we show that the acoustic trapping occurs due to a synergy between hydrodynamic interactions and acoustic primary and interaction forces. The manipulation of submicron particles poses an inherent challenge for methods driven by acoustics. In the Rayleigh limit, i.e., for wavelengths much larger than the particle diameter, the acoustic forces are proportional to the particle volume, while hydrodynamic drag forces are proportional to the particle radius. The trajectories of very small particles, thus, follow the streamlines of the flow (acoustic streaming or imposed background flow), typically limiting the acoustic manipulation to particles larger than a micrometer in diameter [14,15]. In a ground-breaking study, Hammarström *et al.* [4] showed that using either high particle concentrations or preseeding the system with large 10 μm diameter seed particles enables trapping of sub-micron particles, thus overcoming the typical limitation given by the particle size. Originally, Hammarström

et al. [4] hypothesized that the effect could be attributed to either acoustic or hydrodynamic particle-particle interactions; however, no experimental or theoretical verification was shown. In the follow-up studies, Ku *et al.* [11], Broman *et al.* [9], and Costa *et al.* [12] attributed the effect exclusively to acoustic interactions without providing a detailed analysis, while other applied studies avoided discussing the mechanism [6–8]. The dynamics due to many-body interactions can show complex patterns [16], and, despite recent advances in understanding the retention of the seed particle cluster [17–19], and the acoustic particle interactions [20–24], the mechanism of acoustic trapping, especially the interplay between hydrodynamic and acoustic forces, remains unknown [19]. Here, we follow the multibody dynamics approach outlined in [25–27], implemented in MATLAB (2022a and later), to unveil the acoustic trapping mechanism. We model the motion of individual particles driven by an acoustic pressure field and hydrodynamic background flow, taking into account the effect of contacts and of hydrodynamic and acoustic primary and interaction forces. Consider a set of spherical particles placed inside an acoustic field and exposed to a background hydrodynamic flow field. The forces acting on a particle are then the hydrodynamic primary \mathbf{F}_{HYD} , hydrodynamic interaction \mathbf{F}_{HIF} , acoustic primary \mathbf{F}_{ARF} , acoustic interaction \mathbf{F}_{AIF} , and contact forces \mathbf{F}_{CT} . The particle Reynolds number is typically small in microfluidics, and inertial effects can be neglected [25]. Balancing the forces according to Newton's second law then yields [25]

$$\mathbf{F}_{\text{HYD}} + \mathbf{F}_{\text{HIF}} + \mathbf{F}_{\text{ARF}} + \mathbf{F}_{\text{AIF}} + \mathbf{F}_{\text{CT}} = \mathbf{0}. \quad (1)$$

The forces due to the hydrodynamic background \mathbf{F}_{HYD} and particle interactions \mathbf{F}_{HIF} are modeled according to the Stokesian dynamics scheme [28,29]. The primary acoustic

^{*}Contact author: apavlic@caltech.edu

[†]Contact author: Thierry.Baasch@bme.lth.se

radiation force (\mathbf{F}_{ARF}) is given by the negative gradient of the Gor'kov potential [30]. The acoustic interaction forces (\mathbf{F}_{AIF}) are modeled according to Silva and Bruus [31]. The frictionless unilateral contact forces \mathbf{F}_{CT} are modeled using the iterative scheme presented in [25]. The trapping region ($x \in [-130, 130] \mu\text{m}$, $y \in [-187.5, 187.5] \mu\text{m}$) is fully characterized by its hydrodynamic and acoustic background fields. The acoustic field in the trapping region is modeled as a two-dimensional standing wave [17] and given by the pressure p and the velocity field \mathbf{v} :

$$p(x, y, t) = p_a \cos(k_x x) \sin(k_y y) \cos(\omega t), \quad (2)$$

$$\rho_w \frac{\partial}{\partial t} \mathbf{v}(x, y, t) = -\nabla p(x, y, t), \quad (3)$$

where we introduced the pressure amplitude p_a , the fluid density ρ_w , the wave numbers $k_x = (\pi/l)$ and $k_y = (\pi/h)$, the height of the trapping region $h = 375 \mu\text{m}$, the length of the trapping region $l = 260 \mu\text{m}$, and the angular frequency $\omega = 2\pi f$ with $f = 3.5 \text{ MHz}$. The imposed hydrodynamic flow is modeled as a two-dimensional Poiseuille flow in the x direction; formally,

$$v_x(y) = v_{\text{max}} \left(1 - y \frac{2}{h}\right) \left(1 + y \frac{2}{h}\right), \quad (4)$$

where $v_{\text{max}} = 30 \mu\text{m s}^{-1}$ is the velocity along the $y = 0$ plane. We begin the investigation by considering the relative contributions of \mathbf{F}_{HYD} and \mathbf{F}_{ARF} . The acoustic radiation force in the x direction [$F_{\text{ARFx}}(x)$] on a particle placed at $y = 0$ in the acoustic field defined by Eqs. (2) and (3) is given by [17]

$$F_{\text{ARFx}}(x) = -\frac{1}{2} a^3 \kappa_w p_a^2 \frac{k_x k_y^2}{k_x^2 + k_y^2} \sin(2k_x x). \quad (5)$$

The pressure amplitude p_{trap} required to trap a single isolated particle of radius a against a flow of velocity v_{max} and viscosity η along the x direction can be derived by assuming maximal acoustic retention force [i.e., $\sin(2k_x x) = 1$] and performing the force balance according to Eq. (1) with \mathbf{F}_{HYD} and \mathbf{F}_{ARF} , namely,

$$(p_{\text{trap}} a)^2 = 12 \frac{\eta}{f_2 \kappa_w k_x} \left(\frac{k_x^2}{k_y^2} + 1 \right) v_{\text{max}}, \quad (6)$$

where we introduced the dipole scattering coefficient f_2 that is a function of the particle-fluid density ratio [30,32]. The f_2 is positive or negative if the particle is denser or less dense than the surrounding fluid, respectively. The situation is illustrated in Fig. 1(a). The minimum of the Gor'kov potential lies in the center of the trapping region. The cross marks the stable position for a single isolated $5 \mu\text{m}$ polystyrene seed particle in a $p_a = 1.5 \text{ MPa}$ acoustic field

when exposed to a $30 \mu\text{m s}^{-1}$ background flow field. To tease apart the relative importance of acoustic (\mathbf{F}_{AIF}) and hydrodynamic interactions (\mathbf{F}_{HIF}) in acoustic particle trapping, we first look at a few idealized scenarios. Figures 1(b) and 1(c) show the hydrodynamic shielding (S) provided by one [Fig. 1(b)] or a collection of nine seed particles [Fig. 1(c)] to a target particle of $1 \mu\text{m}$ diameter. The shielding is defined as

$$S = 1 - \frac{v_{\text{tg}}}{v_{\text{max}}}, \quad (7)$$

where v_{tg} denotes the velocity of the target particle. At the stable position of a seed particle marked with cross in Fig. 1(a), we study the \mathbf{F}_{AIF} acting on a $1 \mu\text{m}$ target particle in Fig. 1(d). The direction of the acoustic interaction force inverts when the dipole scattering coefficient f_2 of the target particle changes the sign, as shown in Fig. 1(e). Compared to hydrodynamic shielding, the region of influence of the \mathbf{F}_{AIF} is much more confined to the proximity of the seed particle, highlighting the close-range nature of the \mathbf{F}_{AIF} . The amplitude of F_{ARFx} and F_{AIFx} for a seed and target particle placed along the $y = 0$, $z = 0$ line are shown in Fig. 1(f).

Interestingly, at constant center-to-center distance, F_{AIFx} collapses to a single curve when normalized by the volume of the target particle. At constant surface-to-surface distance, smaller target particles experience a larger relative acoustic interaction force.

As many-body interactions drive acoustic trapping (see Supplemental Material [33]), it is necessary to investigate the trapping for an increased number of particles, which makes the analysis more challenging. Therefore, a new parameter, the trapping efficiency η_{trap} , is introduced to quantitatively assess the degree to which particles are retained in the trapping region. Formally, η_{trap} is given by

$$\eta_{\text{trap}} = 1 - \frac{\bar{v}_{x,\text{tg}}}{\bar{v}_{x,\text{ref}}}, \quad (8)$$

where $\bar{v}_{x,\text{tg}}$ denotes the x velocity averaged over all target particles and all times and $\bar{v}_{x,\text{ref}}$ is the average x velocity under reference conditions at $p_a = 0 \text{ MPa}$. A high (1) and low (0) trapping efficiency η_{trap} indicates a strong and weak trapping effect, respectively.

In the numerical multibody dynamic simulations, the particles are initially ($t = 0 \text{ s}$) distributed in an xy grid along the $z = 0$ plane. A jitter proportional to the particle diameters is applied to the particle positions. After release, \mathbf{F}_{ARF} pushes the particles toward the midheight ($y = 0$) plane. The particles are then convected along x with the flow, and, if the applied forces are too weak, the particles will escape the trapping region. Particles passing over the point of maximal force are considered to have escaped. Escaped particles are being extracted from the simulation

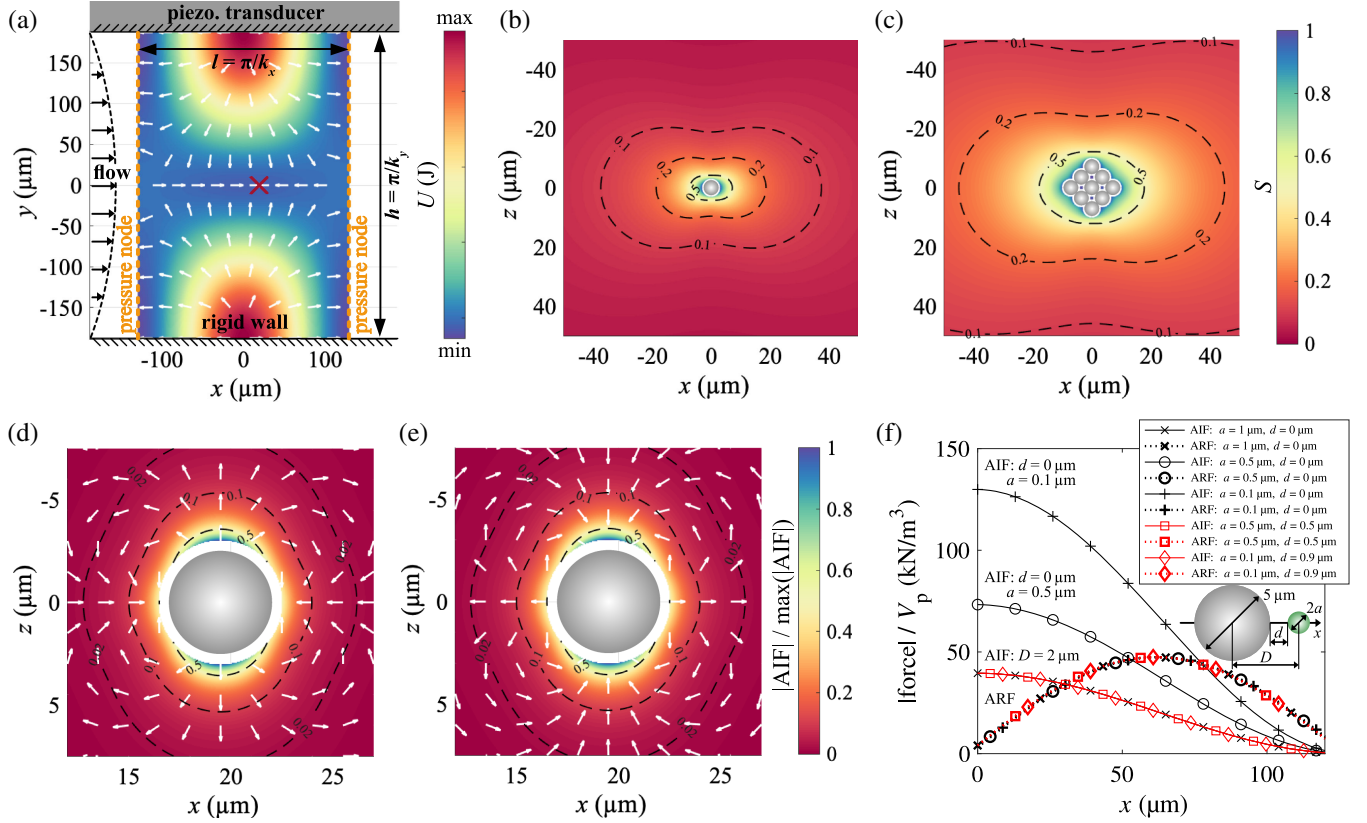


FIG. 1. The 5 μm polystyrene seed particles are trapped in a two-dimensional 1.5 MPa pressure field in water that yields the Gor'kov potential shown in (a). Arrows in (a) indicate the total force on the seed particle, including the hydrodynamic drag from a background Poiseuille flow that reaches $30 \mu\text{m s}^{-1}$ at $y = 0$ and the acoustic radiation force corresponding to the Gor'kov potential. Hydrodynamic shielding from the uniform background flow on a 1 μm target particle provided by (b) a single trapped seed particle or (c) a cluster of nine trapped seed particles. The colors and isolines depict the fraction of the background flow velocity by which the target particle is slowed down, revealing a strong shielding effect near the seed particles. At the stable trapping point of the seed particle along $y = 0$ marked with a cross in (a), we analyze the landscape of acoustic interaction forces on a 1 μm polystyrene target particle in (d) and a modified polystyrene particle with a density of 950 kg m^{-3} and, consequently, a negative dipole scattering coefficient in (e). The color indicates the relative magnitude of the acoustic interaction force acting on the target particle $|AIF|/\max(|AIF|)$, while the arrows indicate the direction. In (f), we move a pair of seed and target particles along the x direction at $y = 0$ and evaluate the ARF and AIF acting on the target particle for different radii of target particles ($a = 1, 0.5, 0.1 \mu\text{m}$), while either the surface-to-surface distance (d) or center-to-center distance are kept constant.

(between $x = 65 \mu\text{m}$ and $x = 75 \mu\text{m}$) and reinjected (between $x = -10 \mu\text{m}$ and $x = 20 \mu\text{m}$) to keep the total number of particles constant. An extensive list of the physical parameters that fully define the numerical experiments is presented in Supplemental Material [33].

First, the trapping efficiency is investigated for 16 monodisperse polystyrene particles from 0.4 to 2 μm diameter in Fig. 2(a), while the acoustic (AIF) and hydrodynamic (HIF) interactions are turned either on or off. The vertical axis at 5.3 is the theoretical prediction obtained from Eq. (6) and indicates the critical product of particle diameter and pressure needed to retain a single isolated particle. The data points cluster into two groups: active F_{HIF} (\square, \diamond , HIF) and inactive F_{HIF} ($+, \times$, noHIF). This indicates that the synergy between F_{ARF} and F_{HIF} dominates the acoustic trapping mechanism of monodisperse

micro- and nanoparticles. This result is not surprising: At close ranges, F_{AIF} is approximately symmetric for a pair of two equal particles. Thus, their contributions cancel for any rigid body motion and do not contribute to the retention of monodisperse particles.

Next, we assess the trapping efficiency as a function of the background pressure for seed particle trapping [Fig. 2(b)]. The diameter of the 12 seed and 13 target particles was set to 5 and 1 μm , respectively, for all cases except for the trapping of nanometer sized target particles, which had a diameter of 500 nm.

Although Brownian motion can impact the motion of submicron particles [29], it is negligible for the presented cases. Indeed, as shown in Fig. 2(b), the mean absolute difference in separation efficiency, including (dashed light blue line) and excluding (light blue line) Brownian motion,

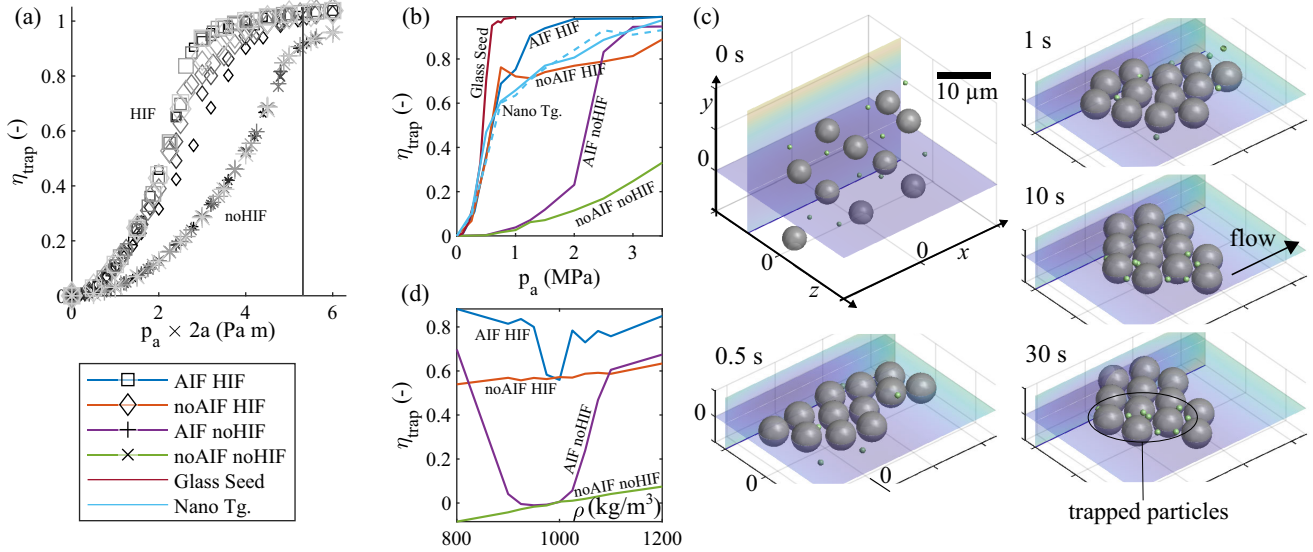


FIG. 2. (a) The acoustic trapping efficiency as a function of the pressure amplitude p_a for 16 monodisperse particles of six different diameters (0.4, 0.6, 0.7, 1, 1.5, and 2 μm). The marker color intensity and size are chosen proportional to the particle size, where a small particle is indicated by a smaller and bolder marker. (b) The acoustic trapping efficiency as a function of the background pressure for acoustic seed particle trapping. The material of the target particles is polystyrene in all cases. The seed particle material is glass in the glass seed case and polystyrene otherwise. Nano Tg indicates 500-nm-diameter target particles. (c) The acoustic trapping of 1 μm polystyrene target particles into a cluster of 5 μm polystyrene seed particles at 1.5 MPa. Both F_{HIF} and F_{AIF} are active. The full video is in Supplemental Material [33]. (d) The impact of the density of the target particles on the trapping efficiency at 1.25 MPa. AIF and HIF indicate the presence, or absence (no), of acoustic and hydrodynamic interactions, respectively. The background flow was a Poiseuille flow with a maximal velocity of 30 $\mu\text{m s}^{-1}$ in all cases. The primary hydrodynamic and acoustic forces were always included. The total simulation times are listed in Supplemental Material [33].

was as small as 0.03. The Brownian motion was, therefore, neglected in all other numerical experiments herein.

Snapshots of the acoustic seed particle trapping at various time points, including the initial constellation at $t = 0$ s, are shown in Fig. 2(c), and the trapping efficiency is summarized in Fig. 2(b). The trapping efficiency was the lowest if both F_{HIF} and F_{AIF} were turned off (noAIF noHIF). Without F_{HIF} (AIF noHIF), the trapping efficiency is low until a critical pressure at which the acoustic interaction forces are sufficiently strong to retain the target particles, and the trapping efficiency experiences a sharp increase as a function of the applied pressure. Without F_{AIF} (noAIF HIF), the trapping efficiency experiences a sharp initial increase exceeding 0.7, which is due to the hydrodynamic shielding from the cluster that is being retained. After the sharp initial increase, the trapping efficiency remains approximately constant. At higher pressure, the cluster moves closer toward the local minimum of the Gor'kov potential ($x = 0$ μm), where the primary acoustic radiation force is weak [see Fig. 1(f)] and, without the support of the AIF, not strong enough to retain the target particles. If all effects are included (AIF HIF), the hydrodynamic interactions provide the collective hydrodynamic shielding, while the acoustic interactions provide an attractive effect even if the cluster is close to the minimum of Gor'kov potential. This synergy allows the efficient trapping of target particles at pressures much lower than

expected from considering acoustically and hydrodynamically isolated target particles (noAIF noHIF). As expected [19], using silica glass seed particles (glass seed) enhances the acoustic interactions and improves the trapping efficiency. Trapping of smaller target particles is still possible (Nano Tg), although the trapping efficiency decreases. As both primary and secondary acoustic radiation forces are dominated by the dipole scattering coefficient f_2 in the trapping region, the trapping efficiency can be tuned by modifying the target particles' f_2 . To showcase this effect, we computed the motion of 16 particles (eight seed and eight target) for various target particle densities at $p_a = 1.25$ MPa. The diameter of the seed and target particles is 5 μm and 750 nm, respectively, and their materials are melamine and density-modified polystyrene, respectively. Figure 2(d) shows the trapping efficiency as a function of the target particle density. As the target particle density approaches the density of the surrounding fluid ($\rho = 1000$ kg m^{-3}), the trapping efficiency drops from 0.88 to 0.56. When the target particles' and buffer's density match, the acoustic forces acting on the target particles vanish. The lower bound to the trapping efficiency is then given by the hydrodynamic interactions, as can be seen from the intersection of the AIF HIF with the noAIF HIF case in Fig. 2(d). The AIF noHIF case shows that trapping due to acoustic interaction forces can be achieved when the particle density is both larger ($f_2 > 0$) and smaller ($f_2 < 0$)

than the density of the surrounding fluid. This indicates that the trapping due to acoustic interactions can occur independently of the acoustic interaction force field orientation, showcased in Figs. 1(d) and 1(e). The trapping efficiency goes to negative values for the noAIF noHIF case if the target particle density is sufficiently small. This is due to the primary acoustic radiation force switching sign and, thus, pushing the target particles out of the trapping region. The results indicate that matching the density of the buffer to the density of the target particles enables density-selective release of target particles.

The mechanism of acoustic trapping is thus explained by the following effects. (i) The collective hydrodynamic shielding provided by the seed particles and the other target particles reduces the effective strength of the background flow. (ii) The ARF is weak close to the equilibrium ($x = 0 \mu\text{m}$), while the AIF remains strong. (iii) The contribution of the AIF to the rigid body motion of a collection of particles is negligible. (iv) The AIF has an attractive component as long as the fluid and target particle densities are not matched.

Acknowledgments—T.B. is supported by the Swedish Research Council (No. 2022-04041), the Crafoordska Stiftelsen (No. 20240891), and the SONOCRAFT project funded by the European Innovation and Research Council (GA: 101187842). A.P. acknowledges support from the Human Frontier Science Program Cross-Disciplinary Fellowship (No. LT0054/2024-C), the Swiss National Science Foundation Postdoc.Mobility Fellowship (No. P500PT_217887), and Mikhail Shapiro.

Data availability—The data that support the findings of this article are openly available [34]; embargo periods may apply.

-
- [1] M. Evander, L. Johansson, T. Lilliehorn, J. Piskur, M. Lindvall, S. Johansson, M. Almqvist, T. Laurell, and J. Nilsson, Noninvasive acoustic cell trapping in a microfluidic perfusion system for online bioassays, *Anal. Chem.* **79**, 2984 (2007).
 - [2] B. Hammarström, M. Evander, H. Barbeau, M. Bruzelius, J. Larsson, T. Laurell, and J. Nilsson, Non-contact acoustic cell trapping in disposable glass capillaries, *Lab Chip* **10**, 2251 (2010).
 - [3] A. Fornell, C. Johannesson, S. S. Searle, A. Hapstadus, J. Nilsson, and M. Tenje, An acoustofluidic platform for non-contact trapping of cell-laden hydrogel droplets compatible with optical microscopy, *Biomicrofluidics* **13**, 044101 (2019).
 - [4] B. Hammarström, T. Laurell, and J. Nilsson, Seed particle-enabled acoustic trapping of bacteria and nanoparticles in continuous flow systems, *Lab Chip* **12**, 4296 (2012).
 - [5] B. Hammarstrom, B. Nilson, T. Laurell, J. Nilsson, and S. Ekstrom, Acoustic trapping for bacteria identification in positive blood cultures with MALDI-TOF MS, *Anal. Chem.* **86**, 10560 (2014).
 - [6] M. Evander, O. Gidlöf, B. Olde, D. Erlinge, and T. Laurell, Non-contact acoustic capture of microparticles from small plasma volumes, *Lab Chip* **15**, 2588 (2015).
 - [7] M. Rezeli *et al.*, Comparative proteomic analysis of extracellular vesicles isolated by acoustic trapping or differential centrifugation, *Anal. Chem.* **88**, 8577 (2016).
 - [8] O. Gidlöf, M. Evander, M. Rezeli, G. Marko-Varga, T. Laurell, and D. Erlinge, Proteomic profiling of extracellular vesicles reveals additional diagnostic biomarkers for myocardial infarction compared to plasma alone, *Sci. Rep.* **9**, 8991 (2019).
 - [9] A. Broman, A. Lenshof, M. Evander, L. Happonen, A. Ku, J. Malmström, and T. Laurell, Multinodal acoustic trapping enables high capacity and high throughput enrichment of extracellular vesicles and microparticles in miRNA and MS proteomics studies, *Anal. Chem.* **93**, 3929 (2021).
 - [10] R. Habibi, V. He, S. Ghavamian, A. De Marco, T.-H. Lee, M.-I. Aguilar, D. Zhu, R. Lim, and A. Neild, Exosome trapping and enrichment using a sound wave activated nano-sieve (SWANS), *Lab Chip* **20**, 3633 (2020).
 - [11] A. Ku, H. C. Lim, M. Evander, H. Lilja, T. Laurell, S. Scheduling, and Y. Ceder, Acoustic enrichment of extracellular vesicles from biological fluids, *Anal. Chem.* **90**, 8011 (2018).
 - [12] M. Costa, L. van der Geer, M. Joaquim, B. Hammarström, S. Tanriverdi, H. Joensson, M. Wiklund, and A. Russom, Echotilt: An acoustofluidic method for the capture and enrichment of nanoplastics directed toward drinking water monitoring, *Micromachines* **15**, 1487 (2024).
 - [13] M. Costa, B. Hammarström, L. van der Geer, S. Tanriverdi, H. N. Joensson, M. Wiklund, and A. Russom, EchoGrid: High-throughput acoustic trapping for enrichment of environmental microplastics, *Anal. Chem.* **96**, 9493 (2024).
 - [14] H. Bruus, Acoustofluidics 10: Scaling laws in acoustophoresis, *Lab Chip* **12**, 1578 (2012).
 - [15] W. Qiu, H. Bruus, and P. Augustsson, Particle-size-dependent acoustophoretic motion and depletion of micro- and nanoparticles at long timescales, *Phys. Rev. E* **102**, 013108 (2020).
 - [16] B. Wu, E. P. Esposito, Q. Mao, and H. M. Jaeger, Pattern formation in acoustically levitated particle systems with competing near-field interactions, *Phys. Rev. Res.* **7**, 023017 (2025).
 - [17] A. Fornell, T. Baasch, C. Johannesson, J. Nilsson, and M. Tenje, Binary acoustic trapping in a glass capillary, *J. Phys. D* **54**, 355401 (2021).
 - [18] M. W. Ley and H. Bruus, Three-dimensional numerical modeling of acoustic trapping in glass capillaries, *Phys. Rev. Appl.* **8**, 024020 (2017).
 - [19] M. Havers, T. Baasch, A. Lenshof, M. Evander, and T. Laurell, Silica seed particles improve the efficiency and throughput of nanoparticle acoustic trapping, *Phys. Rev. Appl.* **21**, 034016 (2024).
 - [20] A. R. Mohapatra, S. Sepehrirahnama, and K.-M. Lim, Experimental measurement of interparticle acoustic radiation force in the Rayleigh limit, *Phys. Rev. E* **97**, 053105 (2018).
 - [21] S. Sepehrirahnama and K.-M. Lim, Generalized potential theory for close-range acoustic interactions in the Rayleigh limit, *Phys. Rev. E* **102**, 043307 (2020).

- [22] D. Saeidi, M. Saghafian, S. Haghjooy Javanmard, B. Hammarström, and M. Wiklund, Acoustic dipole and monopole effects in solid particle interaction dynamics during acoustophoresis, *J. Acoust. Soc. Am.* **145**, 3311 (2019).
- [23] T. Baasch, W. Qiu, and T. Laurell, Gap distance between pearl chains in acoustic manipulation, *Phys. Rev. Appl.* **18**, 014021 (2022).
- [24] A. Pavlic, L. Ermanni, and J. Dual, Interparticle attraction along the direction of the pressure gradient in an acoustic standing wave, *Phys. Rev. E* **105**, L053101 (2022).
- [25] T. Baasch, I. Leibacher, and J. Dual, Multibody dynamics in acoustophoresis, *J. Acoust. Soc. Am.* **141**, 1664 (2017).
- [26] T. Baasch and J. Dual, Acoustofluidic particle dynamics: Beyond the Rayleigh limit, *J. Acoust. Soc. Am.* **143**, 509 (2018).
- [27] A. Pavlic, M. Veljkovic, L. Fieseler, and J. Dual, Acoustophoresis of *Legionella* species in water and the influence of collective hydrodynamic focusing, [arXiv:2211.11508](https://arxiv.org/abs/2211.11508).
- [28] L. Durlofsky, J. F. Brady, and G. Bossis, Dynamic simulation of hydrodynamically interacting particles, *J. Fluid Mech.* **180**, 21 (1987).
- [29] J. F. Brady and G. Bossis, Stokesian dynamics, *Annu. Rev. Fluid Mech.* **20**, 111 (1988).
- [30] L. P. Gor'kov, On the forces acting on a small particle in an acoustical field in an ideal fluid, *Sov. Phys. Dokl.* **6**, 773 (1962).
- [31] G. T. Silva and H. Bruus, Acoustic interaction forces between small particles in an ideal fluid, *Phys. Rev. E* **90**, 063007 (2014).
- [32] H. Bruus, Acoustofluidics 7: The acoustic radiation force on small particles, *Lab Chip* **12**, 1014 (2012).
- [33] See Supplemental Material at <http://link.aps.org/supplemental/10.1103/6l7z-bjzy> for an analysis of the many-body effect.
- [34] A. Pavlic and T. Baasch, Zenodo repository, [10.5281/zenodo.15575920](https://zenodo.org/record/15575920), version 1 (2025).